Multiwalled Carbon Nanotubes Coated with Tungsten Disulfide

Raymond L. D. Whitby,[†] Wen Kuang Hsu,[†] Peter K. Fearon,[†] Norman C. Billingham,[†] Isabelle Maurin,[†] Harold W. Kroto,[†] David R. M. Walton,*[,†] Christopher B. Boothroyd,[‡] Steven Firth,[§] Robin J. H. Clark,[§] and David Collison[||]

School of Chemistry, Physics and Environmental Science, University of Sussex, Brighton BN1 9QJ, United Kingdom, Department of Materials Science and Metallurgy, University of Cambridge, Pembroke Street, Cambridge CB2 3QZ, United Kingdom, Christopher Ingold Laboratories, University College London, 20 Gordon Street, London WC1H 0AJ, United Kingdom, and EPSRC National Service for cwEPR Spectroscopy, Chemistry Department, The University of Manchester, Manchester, M13 9PL, United Kingdom

Received November 21, 2001. Revised Manuscript Received February 14, 2002

Novel binary-phase WS_2−C nanotubes were generated by pyrolyzing WO_3-coated multiwalled carbon nanotubes in an H_2S/N_2 atmosphere at 900 °C. The WS_2 coating acts as an anti-oxidizing agent.

Introduction

Rothschild et al. recently produced WS_2 nanostructures by pyrolyzing H_2S in the presence of tungsten carbide.[1] In earlier processes,[2,3] WO_3 particles were reduced to WO_{3-x} ($x = 0.1-0.5$)[4] by being heated at 800−900 °C in the presence of H_2/H_2S, and then to WS_2 on the particle surface.[3] S rapidly replaces O at the WO_{3-x} surface to form 1−2 layers of WS_2.[2,3] Finally, H_2S diffuses toward the center of the particle via lattice vacancies and the formation of WS_2 internal layers continues. This reaction sequence was verified by several observations: (a) the encapsulation of WO_{3-x} within WS_2 shells, which implies incomplete WO_{3-x} to WS_2 conversion;[4] (b) the thickening of the WS_2 walls when pyrolysis in H_2S is prolonged; (c) the similarity of the dimensions of the resulting WS_2 nanostructures to those of the WO_3 precursors.[2,3] The WO_3 to WS_2 conversion is therefore a template process,[2,3] in that the WS_2 morphology is closely controlled by that of the original WO_3 material.

Zhu et al. have recently carried out related experiments using monoclinic WO_2 as a precursor and found that it can easily be converted into hexagonal WS_2,[5,6] apparently more readily than can WO_3. The reaction can be expressed as

$$WO_2 + 2H_2S \rightarrow WS_2 + 2H_2O$$

with no intermediate WO_{3-x} being involved. Tungsten in WO_2 and WS_2 has the same oxidation state and electronic configuration [M^{IV}, $(Xe)4f^{14}5d^2$] and the substitution of O by S requires a substantial lattice expansion (ca. 2.7 Å) along the O−W−O (011) plane direction, leading to (002) S−W−S basal plane formation (ca. 6.2 Å *d* spacing). The lattice expansion results in a density reduction from WO_2 (10,800 kg m^{-3}) to WS_2 (7,500 kg m^{-3}). By contrast in the process WO_3 to WS_2, the substitution of O by S involves a structural change, in particular the formation of the intermediate WO_{3-x}, crystallographic shear[4] and oxygen vacancies in the WO_{3-x} lattice.[4]

In this work, we have studied the conversion of WO_3 into WS_2 on the surface of multiwalled carbon nanotubes (MWCNs). This study indicates that the formation of WS_2 can occur on nonplanar substrates, particularly at the MWCN tips. This process involves two steps: WO_3 coating of MWCNs, followed by H_2S pyrolysis. It is known that the wetting of MWCN surfaces is difficult.[7] The previous methods for coating MWCNs with WO_3[8,9] involved their oxidation, which generated surface

* To whom correspondence should be addressed. E-mail: d.walton@sussex.ac.uk.
[†] School of Chemistry, Physics, and Environmental Science, University of Sussex.
[‡] Department of Materials Science and Metallurgy, University of Cambridge.
[§] Christopher Ingold Laboratories, University College London.
[||] EPSRC National Service for cwEPR Spectroscopy.

(1) Rothschild, A.; Sloan, J.; York, A. P. E.; Green, M. L. H.; Hutchison, J. L.; Tenne, R. *Chem. Commun.* **1999**, 363.
(2) Feldman, Y.; Frey, G. L.; Homyonfer, M.; Lyakhovitskaya, V.; Margulis, L.; Cohen, H.; Hodes, G.; Hutchison, J. L.; Tenne, R. *J. Am. Chem. Soc.* **1996**, *118*, 5362.
(3) Rothschild, A.; Sloan, J.; Tenne, R. *J. Am. Chem. Soc.* **2000**, *122*, 5169.
(4) Sloan, J.; Hutchison, J. L.; Tenne, R.; Feldman, Y.; Tsirlina, T.; Homyonfer, M. *J. Solid State Chem.* **1999**, *144*, 100.
(5) Zhu, Y. Q.; Hsu, W. K.; Grobert, N.; Chang, B. H.; Terrones, M.; Terrones, H.; Kroto, H. W.; Walton, D. R. M.; Wei, B. Q. *Chem. Mater.* **2000**, *12*, 1190.
(6) Zhu, Y. Q.; Hsu, W. K.; Terrones, H.; Grobert, N.; Chang, B.; Terrones, M.; Wei, B. Q.; Kroto, H. W.; Walton, D. R. M.; Boothroyd, C. B.; Kinloch, I.; Chen, G. Z.; Windle, A. H.; Fray, D. J. *J. Mater. Chem.* **2000**, *10*, 2570.
(7) Dujardin, E.; Ebbesen, T. W.; Hiura, H.; Tanigaki, K. *Science* **1994**, *265*, 1850.
(8) Satishkumar, B. C.; Govindaraj, A.; Nath, M.; Rao, C. N. R. *J. Mater. Chem.* **2000**, *10*, 2115.
(9) Hsu, W. K.; Zhu, Y. Q.; Kroto, H. W.; Walton, D. R. M.; Kamalakaran, R.; Terrones, M. *Appl. Phys. Lett.* **2000**, *77*, 4130.

10.1021/cm011282k CCC: $22.00
Published on Web 04/20/2002

−COOH or −OH groups.[9] The MWCNs, however, were uncapped and peeled.[9] Here we describe a technique for depositing WO_3 on MWCN surfaces without peeling or uncapping the MWCNs during the conversion of WO_3 into WS_2.

Experimental Section

The MWCNs were prepared by dc arc vaporization of graphite rods in a He atmosphere (500 Torr) at 20 V, 80−100 A. The MWCNs were removed from the cathode deposit and were not purified further. The MWCN and carbon particle ratio is ca. 3:1. The WS_2-coated MWCNs were produced as follows. H_2WO_4 (250 mg) and MWCNs (50 mg) were mixed at −78 °C in liquid NH_3 (∼20 cm^3) and the mixture was set aside in order to attain room temperature. The solid residue was then heated at 350 °C for 15 min in an air flow (100 cm^3 min^{-1}) in order to convert H_2WO_4 into WO_3 (and to remove simultaneously any amorphous carbon which may be coating the MWCNs). The material at this stage contains: (a) WO_3 particles; (b) MWCNs coated with amorphous material; and (c) clean MWCNs. An EDX analysis of (b) revealed the presence of C, W, and O arising from both the MWCNs and the amorphous coating, suggesting that the amorphous material coating the MWCNs is WO_{3-x} ($x = 0$ to 1).

WO_{3-x}-coated MWCNs were then heated at 900 °C in N_2/H_2S (3:1 ratio, 50 cm^3 min^{-1} total flow rate) for 10 min. The products were ultrasonically dispersed in acetone and mounted on lacey carbon films (Cu support grids) for TEM analysis. The following equipment was employed as appropriate: HRTEM (JEOL JEM 4000 EX II operated at 400 kV, Philips CM 200 operating at 200 kV) equipped with an energy-dispersive X-ray probe and line mapping (EDX), X-ray diffraction (XRD, Siemens diffractometer D5000, Cu Kα = 1.5418 Å), EPR (Bruker ESP 300E and EMX), TGA (Perkin-Elmer TGA-7, heating rate of 10 K min^{-1}) and Raman (Renishaw System 1000).

Results and Discussion

HRTEM and EDX Analyses. After treatment with H_2S, the product was found to consist of MWCNs (ca. 60%) either partly or completely coated with a layered material. The coating layers exhibited a darker fringe contrast than the MWCNs and, typically, consisted of 1−4 layers parallel to the basal planes of the MWCNs. Amorphous material was occasionally seen attached to the coating layers, and polyhedral particles were observed with similar coatings to those on the MWCNs. There is a ca. 4.4 Å spacing between each MWCN and the coating layer, a value which remains more or less constant in all observed coated structures. The layer-intact MWCN structures display no significant surface damage other than variation in their 3.4 Å *d* spacing. Typical examples are shown in Figure 1: (a), (b), and (c) in which MWCNs with an incomplete single-layer coating, a full single-layer coating, and a double-layer coating, respectively, are depicted. Figure 1d shows a single-layer coating at the tube tip and Figure 1e a partly coated carbon particle.

EDX analyses were carried out on bare, partly coated, and fully coated MWCNs. The bare MWCNs show only a C signal (Figure 2a). The fully coated MWCNs reveal the presence of C, W, and S, together with a trace of O (Figure 2b). The presence of small quantities of O may arise from the amorphous coating (Figure 1a), i.e. residual WO_{3-x}. Two different EDX spectra were observed for partly coated MWCNs. First, only a C peak was present when the EDX probe was focused on the uncoated areas of the MWCNs. Second, W, C, and S peaks were detected when the probe was focused on the coated areas of the MWCNs. A trace of O was occasionally detected in the partly coated area. Quantitative analysis showed the W:S ratio is ca. 1:2 (±0.1), implying a WS_2 structure. EDX also revealed that the large dark-layered particles are WS_2, formed via the process: $H_2WO_4 \rightarrow WO_3 \rightarrow WS_2$. EDX analyses were also carried out on the amorphous material coating the MWCNs, prior to H_2S pyrolysis. C, W, and O were detected (Figure 2c,d), which indicates that H_2WO_4 had been converted into amorphous WO_3 and deposited on the MWCN surfaces. It is noteworthy that the sample had been heated at 350 °C for 15 min in air, which had removed the initial amorphous carbon coating MWCNs. Accordingly, the amorphous coating seen in Figure 2d is WO_3.

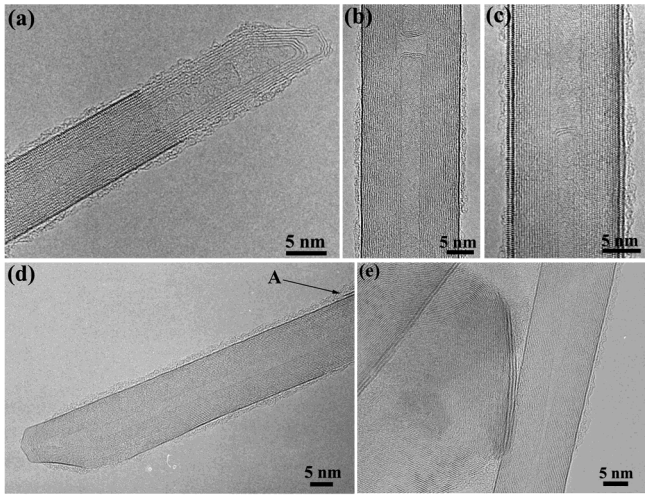

Figure 1. HRTEM images of (a) partly single-layer WS_2-coated MWCN, (b) fully single-layer WS_2-coated MWCN, (c) fully double-layer WS_2-coated MWCN, (d) single-layer WS_2-coated MWCN tip (including an external terminating WS_2 layer, arrow A), and (e) partly WS_2-coated carbon particle.

EDX Mapping Analysis. The tilting of partly WS_2-coated MWCNs (ca. ±25°) occasionally shows small WS_2 fringe variations along the tube axis. Figure 3a shows that the WS_2-coated MWCNs are not always uniform, i.e. one side is thicker than the other. Figure 1a shows that the WS_2 coating of this tube is essentially uniform, but that its termination edge is irregular. Such a pattern is not found for fully WS_2-coated MWCNs. In Figure 3b, the MWCN was coated with WS_2 on one side only (arrow B). Two features of this image are noteworthy. First, the MWCN-layered fringes are clearly seen in the uncoated area (arrow A), whereas interference of WS_2 and MWCN fringes is present in the coated area (arrow B). Second, the fringe interference is also seen in the MWCN central core region (white arrow and lines), which indicates that the WS_2 coating covers at least half of the MWCN circumference (insert, Figure 3b). When the incident beam passes through the partly WS_2-coated MWCN, the section of the WS_2 coating parallel to the incident beam results in 002 fringe formation on one side only (arrow B, Figure 3b). The presence of WS_2 and MWCN fringe interference in the central region arises from the basal planes of WS_2 and MWCNs, perpendicular to the incident beam.

EDX mapping analysis was carried out on a double-walled WS_2-coated MWCN (Figure 3c). The C, W, and S mappings were taken from C Kα, W $M\alpha_1$, and S Kα

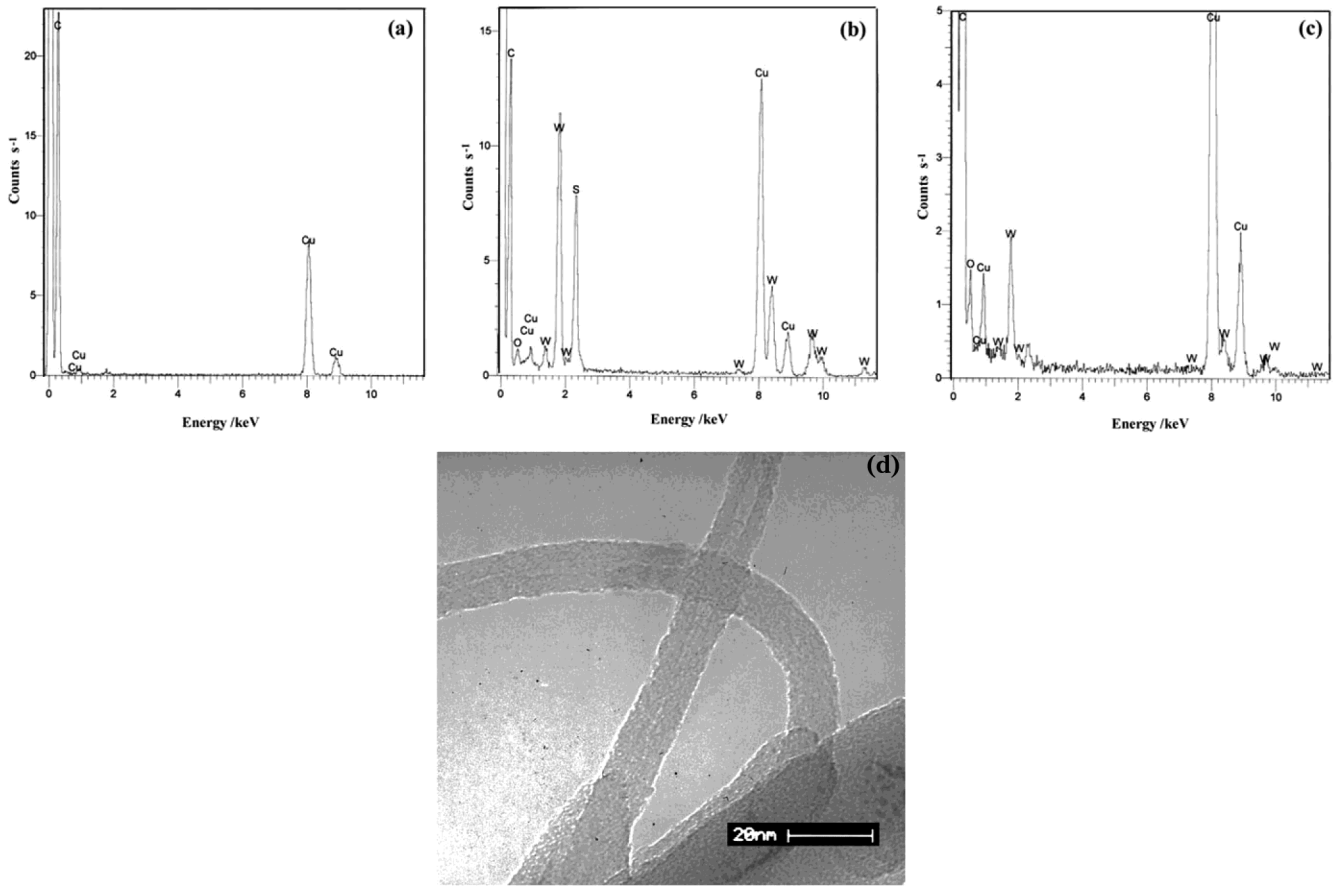

Figure 2. (a) EDX profiles for uncoated MWCNs, (b) WS_2-coated MWCNs, (c) WO_3-coated MWCNs, and (d) WO_3-coated MWCN.

states, respectively. The mapping profile intensity follows the sequence W > S > C. The width of the C profile (rodlike feature, top, Figure 3c) is less (by ca. 10 nm) than those of the W (middle) and S profiles (lower), which are the same. The TEM tilting and mapping analyses clearly indicate that the MWCNs are actually sheathed within WS_2 tubes.

Electron Diffraction (ED) Analysis. The difficulty in analyzing the ED pattern of WS_2-coated MWCNs arises because the MWCN spot arrays partly overlap those of WS_2, and because the MWCNs selected do not always possess a uniform coating of WS_2, a problem which can be overcome by tilting the MWCNs. Differentiating between overlapping MWCN and WS_2 spot arrays was achieved by comparison of the observed ED pattern with a computer simulation. Figure 4a shows the ED pattern of a MWCN coated with double-walled WS_2. Only WS_2 spots are indexed, together with (0002) MWCN spots. The MWCN side-wall (0002) diffraction spots are stronger and have larger spacing than those of WS_2, due to their smaller layer separation (3.4 Å) and to the presence of additional C-shells. The indexed WS_2 spots appear to be arranged in a double-hexagonal pattern (Figure 4b). Each hexagon corresponds to in-plane diffraction of the front (or rear) WS_2 shell. The angle between the tube axis and the hexagon is ca. 9° (Figure 4b); i.e. the WS_2 coating is a 9° helical tube. The unindexed spots, which belong to the MWCNs, are very weak due to strong dispersion. Computer simulations do not match with the MWCN spots perfectly, but imply that the encapsulated C-shells do not have identical chirality to the WS_2 coating.

X-ray Diffraction Measurements. As a result of pyrolyzing H_2S over WO_3-coated MWCNs, the mass of the final material increased by ca. 7%. This value includes the separate WS_2 nanostructures as well as WS_2-coated MWCNs. The mass of amorphous carbon initially attached to the MWCN surface and subsequently removed by oxidation is negligible. The X-ray diffraction pattern of the WS_2-coated MWCN sample is shown in Figure 5 . The MWCN reflections mostly overlap with those of WS_2. The WS_2 reflection intensity is significantly greater than that displayed by the MWCNs. The only reflection arising from the coated-MWCNs corresponds to the (002) line at ca. $2\theta = 26.5°$, similar to that of uncoated-MWCNs.[10] The (002) reflection of MWCNs slightly shifts to the lower angle by ca. 2−4%, as compared with graphite. However, the unchanged MWCN 002 peak position indicates that the WS_2 coating does not lead to much distortion of the MWCN shells. From the full width at half-maximum (fwhm) of the WS_2 (002) reflection, the number of WS_2 layers along the *c*-axis is estimated to be ca. 5. This number is a mean value for independent WS_2 particles (ca. 4−10 layers) and WS_2-coated MWCNs (ca. 1−3 layers).

The X-ray diffraction pattern reveals that WS_2 has a well-developed crystalline structure. For example, the intensities of the (001) reflections (002, 004, 006), "in-plane" reflections (100, 110) and "3D reflections" (101, 105) are relatively strong, as compared with those of pure WS_2 nanotubes and bulk WS_2.[6] Therefore, it is not only possible but likely that the XRD pattern is mostly generated by other separate WS_2 nanostructures with

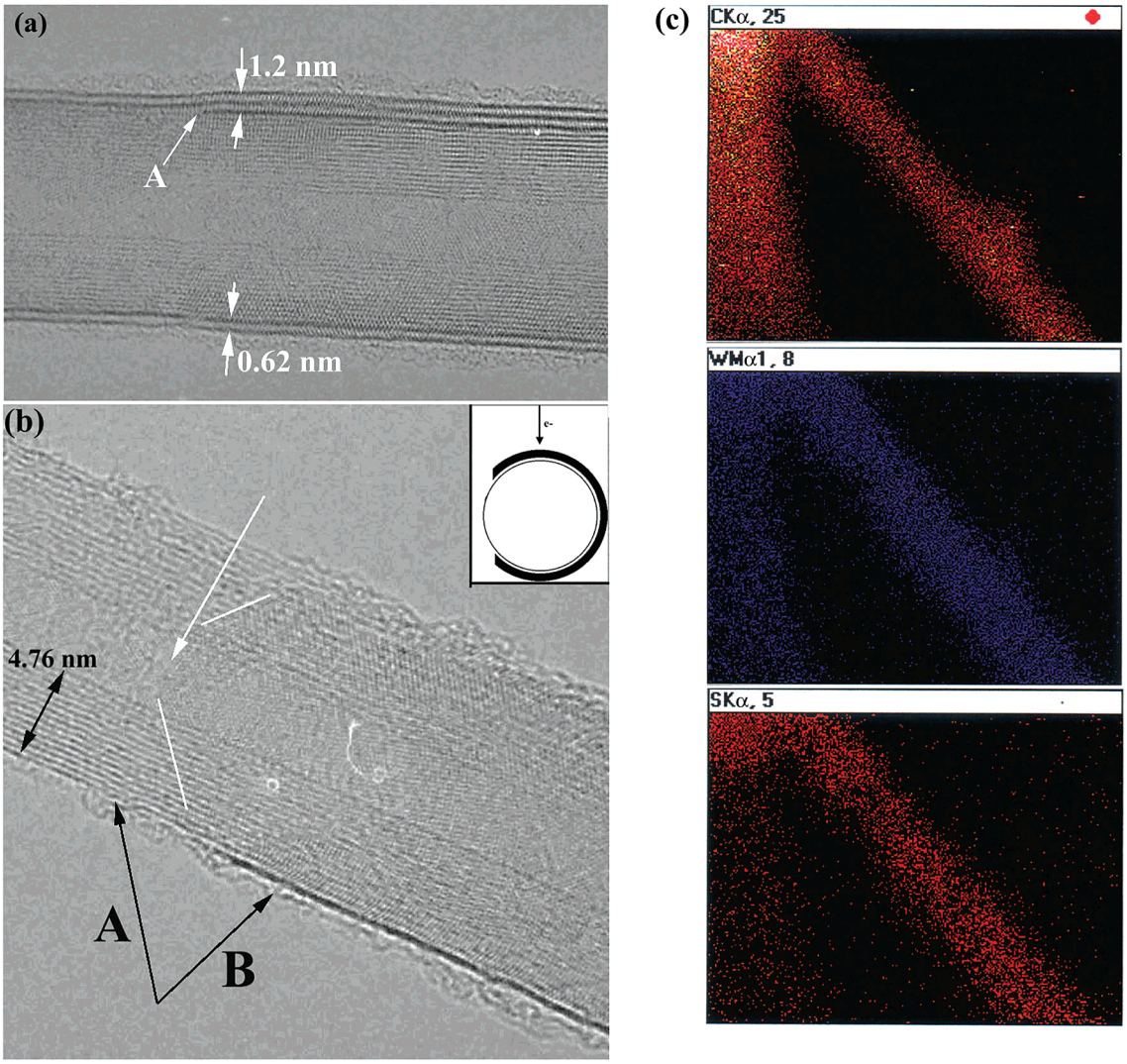

Figure 3. HRTEM image of (a) a WS_2-coated MWCN exhibiting encapsulation of a terminating WS_2 layer (Arrow A) and (b) the termination edge of a WS_2 layer observed on a partially WS_2-coated MWCN (left of white lines). Insert shows a model of an incompletely closed WS_2 layer in the electron beam. (c) EDX mapping analysis reveals the distribution of C, W, and S in a WS_2-coated MWCN.

only small diffraction components arising from the WS_2 coatings.

Raman Spectroscopy. Raman spectra, recorded at room temperature and at excitation wavelengths 514.5 and 632.8 nm, are shown in Figure 6a,b, respectively. For each wavelength, the spectrum consists of bands below 833 cm^{-1} associated with WS_2 and two broad bands above 1300 cm^{-1} associated with MWCNs. The relative intensities of the two sections of the spectrum vary with excitation wavelength and, in particular, the spectrum of WS_2 is enhanced by a 632.8 nm excitation. Resonance enhancement also accounts for the greater number of bands observed below 900 cm^{-1} in the 632.8 nm spectrum. The G- and D-bands of MWCNs are weak and broad (bandwidths at half-height ca. 90 cm^{-1}); therefore the intensity ratio, I_G/I_D, is difficult to measure. The wavenumber of the G-band of the WS_2-coated MWCNs (1585 cm^{-1}) is identical for both 514.5 and 632.8 nm excitation and is ca. 14 cm^{-1} higher than that for uncoated MWCNs.[10,11] This increase may be due to the WS_2 coating, which constrains the C−C vibrations of the MWCNs. The D-band of WS_2-coated MWCNs in the 514.5 nm spectrum is also higher than that for uncoated MWCNs, possibly for the same reason as that given above for the increase in the G-band wavenumber (Figure 6a). In the 632.8 nm spectrum, the D-band wavenumber is 1323 cm^{-1} (Figure 6b), ca. 43 cm^{-1} lower than the value seen in the 514.5 nm spectrum. This decrease in D-band wavenumber with increased excitation wavelength is substantially larger than those reported previously (ca. 14 cm^{-1} for MWCNs[11] and 28 cm^{-1} for boron-doped MWCNs[10]). The large decrease in the wavenumber of the D-band is due to resonance enhancement at different points on the Brillouin zone edge with different excitation lines, the large decrease seen here implying that the electronic structure of MWCNs has been slightly altered, either by the WS_2 coating or by a thin WO_{3-x} deposit. The latter is the more likely, because WS_2 lies 4.4 Å above the MWCN surface.

The observed spectra of WS_2 are similar to those previously reported by Frey et al.[12] There is a weak band

(10) Hsu, W. K.; Firth, S.; Redlich, P.; Terrones, M.; Terrones, H.; Zhu, Y. Q.; Grobert, N.; Schilder, A.; Clark, R. J. H.; Kroto, H. W.; Walton, D. R. M. *J. Mater. Chem.* **2000**, *10*, 1425.

(11) Bacsa, W. S.; e Heer, W. A.; Ugarte, D.; Chatelain, A. *Chem. Phys. Lett.* **1993**, *211*, 346.

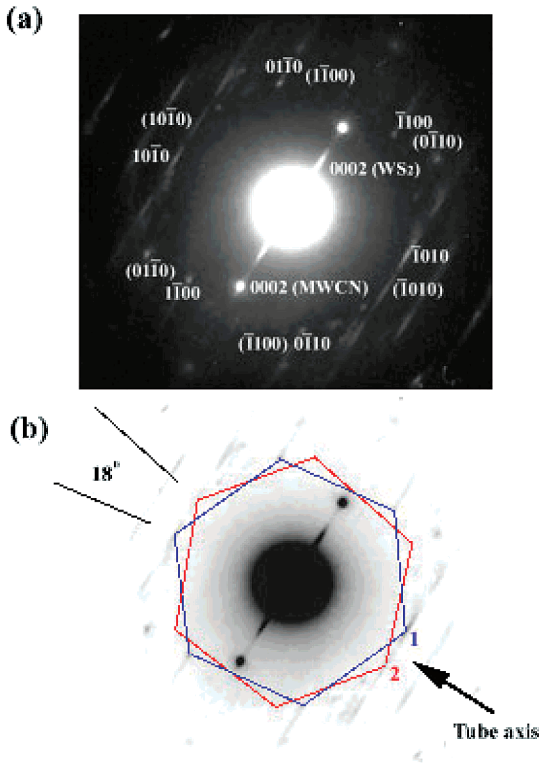

Figure 4. (a) An indexed electron diffraction pattern of a double WS_2-coated MWCN. The $\{10\bar{1}0\}$ diffraction spots from the front and rear WS_2 surfaces are indexed (indices from one surface are in parentheses), as are the (0002) spots from the WS_2 and from the MWCN. (b) A model depicting the hexagonal structure of the WS_2-coated MWCN as determined from a color inverted image of the ED pattern.

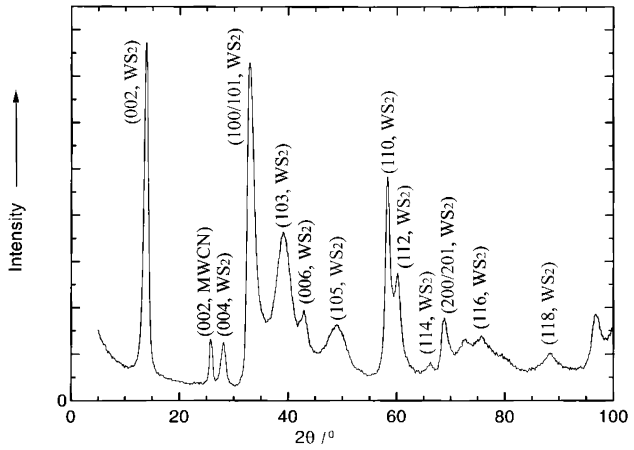

Figure 5. XRD profile of a sample containing WS_2-coated MWCNs.

at 155 cm^{-1} in the 632.8 nm excitation spectrum, which does not appear in the spectrum of bulk WS_2. In our sample, the presence of separate large WS_2 particles, similar to planar flakes, would not give rise to a band at 155 cm^{-1}.[12] This band arises from folding the Brillouin zone along the Γ-M edge, due to the formation of fullerene- and nanotube-like structures.[12] We therefore conclude that the WS_2 coatings are responsible for the presence of the 155 cm^{-1} band. We also carried out

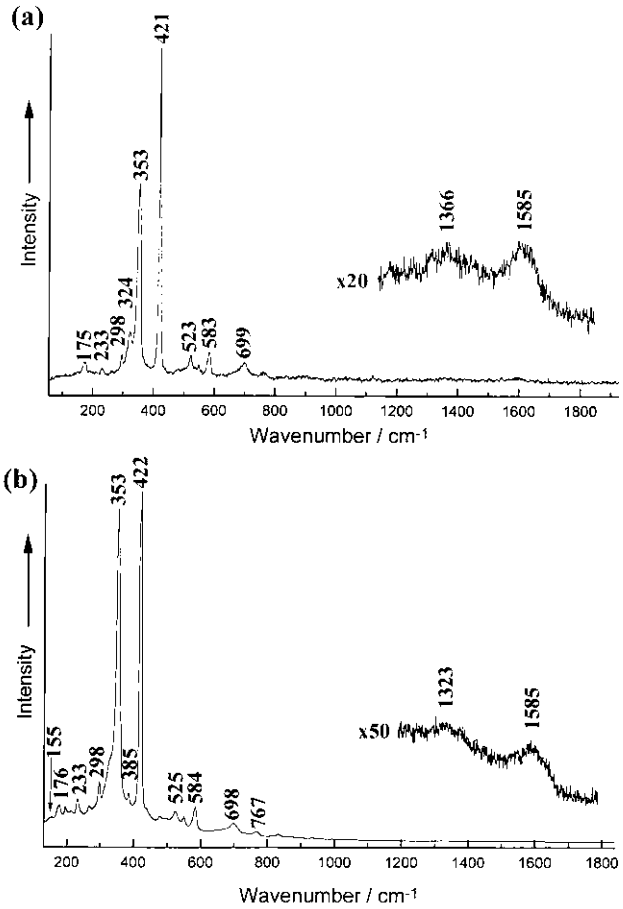

Figure 6. Raman spectra of WS_2-coated MWCNs obtained using (a) 514.5 nm and (b) 632.8 nm excitation. Inserts are magnifications of the spectra to show the D- and G-bands of MWCNs.

Raman measurements on WO_3-coated MWCNs and it was found that the Raman bands of coated MWCNs are the same as those of the uncoated ones above 1000 cm^{-1}.

Electron Paramagnetic Resonance and SQUID Measurements. *X-Band EPR Measurements.* The sample contains three components: (a) independent WS_2 particles, (b) MWCNs, and (c) WS_2-coated MWCNs. An EPR signal from conduction electrons can only be detected when the carbon nanotubes are metallic or narrow band gap semiconductors (<0.1 eV).[13,14] The WS_2 nanostructures are semiconductors, exhibiting a 1.3 eV indirect band gap and a 2.05 eV direct band gap[15] and therefore the detection of conduction electrons is not expected. The EPR spectra (10−290 K) of WS_2-coated MWCNs are shown in Figure 7.

A wide field sweep (9.1 GHz excitation) at room temperature gave an apparently axial spectrum at ca. $g = 2$, with the lower field component more intense, and no other features up to 7 kG. Spectra collected at 10, 20, 40, and 60 K (9.5 GHz excitation) show that there are two distinct signals in the "$g = 2$" region (Figure 7), with a pair of weaker and broader features to lower field at 3240 and 3260 G. The narrower signal (B) at higher

(12) Frey, G. L.; Tenne, R.; Matthews, M. J.; Dresselhaus, M. S.; Dresselhaus, G. *J. Mater. Res.* **1998**, *13*, 2412.

(13) Kosaka, M.; Ebbesen, T. W.; Hiura, H.; Tanigaki, K. *Chem. Phys. Lett.* **1994**, *225*, 161.

(14) Kosaka, M.; Ebbesen, T. W.; Hiura, H.; Tanigaki, K. *Chem. Phys. Lett.* **1995**, *233*, 47.

(15) Frey, G. L.; Elani, S.; Homyonfer, M.; Feldman, Y.; Tenne, R. *Phys. Rev. B* **1998**, *57*, 6666.

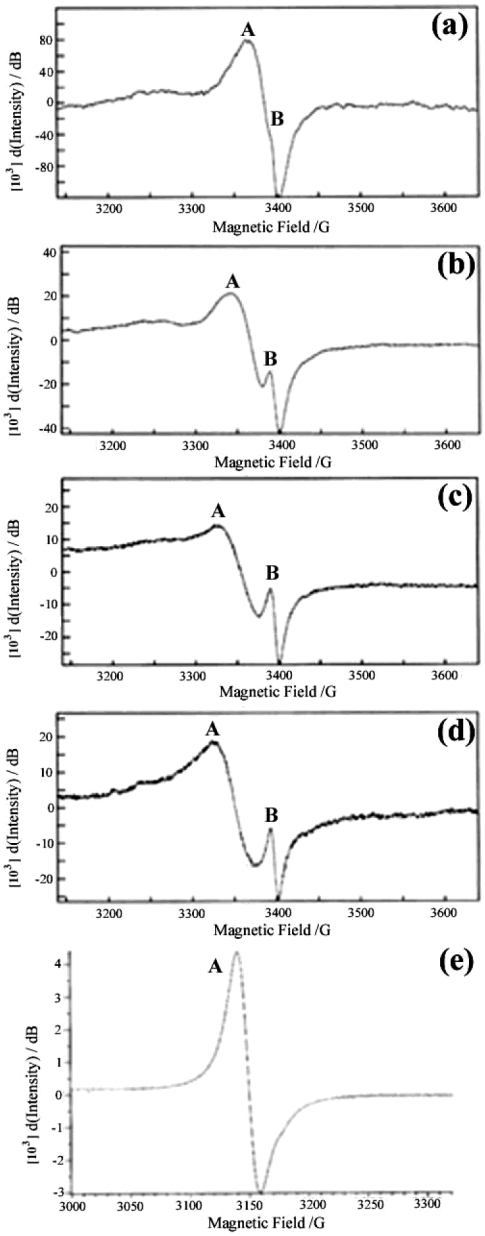

Figure 7. (a)−(e) EPR measurements of WS_2-coated MWCNs conducted at 10, 20, 40, 60, and 290 K, respectively.

field, centered on ca. 3400 G ($g \approx 2.001$, $\Delta B \approx 9$ G), is relatively unchanged throughout the temperature range 60−20 K. The lower field signal (A) is the more intense, but moves significantly upfield and narrows as the temperature is lowered, overlapping with the signal at $g \approx 2.001$ at 10 K. The two weaker lower field features do not vary with temperature, and it is not clear whether they are associated with the broader major resonance. As the temperature is raised from 100 to 295 K signal A progressively broadens, becomes more intense, and moves downfield allowing signal B to become more apparent. Low temperature (10−60 K) measurement at the Q-band frequency revealed no additional information because of the extreme ease with which the signal was saturated.

The major feature A in the X- band spectrum recorded at room temperature appears identical to that previously reported for MWCNs.[13,14] Peak B at low temperature shows features arising from lattice defects, either

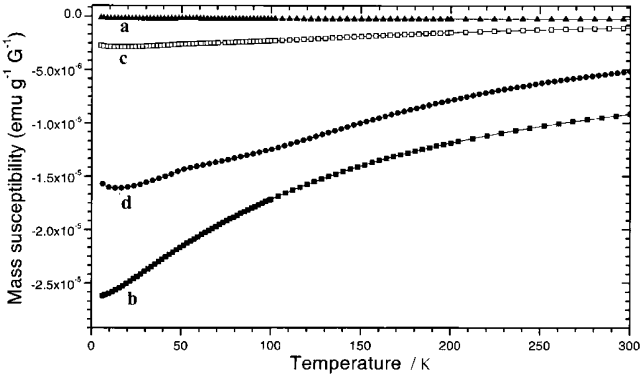

Figure 8. SQUID measurements at 5000 G of (a) WS_2 nanostructures, (b) MWCNs, and (c) WS_2-coated MWCN sample. (d) shows the contribution arising from bare and coated MWCNs in (c).

from uncoated and coated MWCNs or from separate polyhedral carbon particles.

SQUID Measurements. dc magnetization measurements were carried out with a commercial SQUID magnetometer using gelatine capsules as sample holders. The contribution of the capsules, ca. 10^{-7} emu g^{-1} G^{-1}, was subtracted from the raw data. Figure 8 shows the results of field-cooled magnetization measurements at 5000 G for WS_2 nanostructures (curve a), MWCNs (curve b), and WS_2-coated MWCNs (curve c). The mass susceptibility of the WS_2 nanostructures shows a temperature independent diamagnetic behavior, $\chi_m \sim -2.0 \times 10^{-7}$ emu g^{-1} G^{-1}, as previously reported.[16] An additional paramagnetic Curie tail is apparent below 50 K. On the other hand, the MWCNs exhibit a large diamagnetic response, also in agreement with previous reports.[17,18] This large diamagnetism arises from inter-band transitions similar to those in graphite, indicating that most of the tubes are metallic or narrow band gap structures. The coated-MWCNs (curve c) show a significantly reduced susceptibility over the whole temperature range, as compared to bare MWCNs. This is primarily due to the presence of large amounts of independent WS_2 nanostructures in the sample.

The contribution arising from the MWCNs was therefore extracted by subtracting the response of WS_2 using curve a) weighted to correspond to the mass fraction of the precursor in the synthesis process. The resulting curve d shows a reduced susceptibility as compared to those of bare MWCNs (curve b) and a Curie-type tail. (Note that the susceptibility decrease for WS_2-coated MWCNs is here underestimated, as the fraction of coated MWCNs, determined by HRTEM, is ca. 60%.) This susceptibility change indicates a loss of metallic character, possibly associated with a substantial reduction of carrier density and/or mobility, due to localization effects on the structural defects. This is consistent with the presence of a large Curie-type paramagnetic contribution (due to localized electron spins), which sug-

(16) Lévy, F. *Intercalated Layered Materials*; Reidel Publishing, D.; Dordrecht, 1979; p 117.
(17) Ramirez, A. P.; Haddon, R. C.; Zhou, O.; Fleming, R. M.; Zhang, J.; McClure, S. M.; Smalley, R. E. *Science* **1994**, *265*, 84.
(18) Hsu, W. K.; Chu, S. Y.; Munoz-Picone, E.; Boldu, J. L.; Firth, S.; Franchi, P.; Roberts, B. P.; Schilder, A.; Terrones, H.; Grobert, N.; Zhu, Y. Q.; Terrones, M.; McHenry, M. E.; Kroto, H. W.; Walton, D. R. M. *Chem. Phys. Lett.* **2000**, *323*, 572.

gests that the WS_2 coating process has introduced crystalline defects into the MWCN structure, possibly due to WS_2 compression on the MWCN layers or oxidation damage during sample synthesis.

TGA Analysis. For comparative purposes, TGA analyses were performed on MWCNs, WS_2 nanostructures (including nanotubes and nanoparticles), and WS_2-coated MWCNs. The WS_2 nanostructures were produced by a method similar to that described previously.[6] The oxidation of MWCNs in air has been well-documented;[19] for example MWCNs undergo ca. 99% mass loss on being heated at 750 °C for 30 min. The remaining 1% are significantly damaged and decapped.[19]

In Figure 9 (a), the TGA curve of MWCNs (red line) shows that their oxidation begins at ca. 700 °C, and drastic mass loss occurs between 700 and 900 °C. At ca. 910 °C, their mass loss is ca. 99%, consistent with a previous report.[19]

The TGA curve showing oxidation of WS_2 nanostructures (green line) exhibits a 3% mass loss at ca. 530 °C, attributed to their partial reconversion to WO_3 and resulting in a light-green powder. No further mass loss occurs in the 500−950 °C range. The TGA curve of WS_2-coated MWCNs (blue line) shows a stepwise profile. A mass loss at 450 °C is attributed to the onset of conversion of WS_2 into WO_3. Between 450 and 550 °C, the mass loss is ca. 8%; a small mass loss (2%) occurs between 550 and 700 °C. From 700 to 830 °C, the mass loss is ca. 30%; no further mass loss is recorded above 830 °C, although the sample changed from black to dark-green. The residue was analyzed by TEM and EDX. TEM revealed the presence of MWCNs and particles, which have suffered minimal surface damage (Figure 9b). The oxidation of MWCNs results in tapered tubes (Figure 9b, arrows) due to peeling. TEM also revealed the presence of a very thin amorphous coating (<1 nm thick; possibly WO_3) on MWCN surfaces. Larger WO_3 particles, probably originating from the initial oxidation prior to H_2S pyrolysis, are also present (Figure 9b). EDX of oxidized MWCNs revealed the presence of W, C, and O, but no S. According to TEM and EDX analyses, the WS_2 coating delays the oxidation of MWCNs via WS_2 to WO_3 conversion. First, when the temperature reaches 450 °C, the WS_2 coating begins to convert into WO_{3-x}. This process is similar to that of WS_2 nanostructures (green line), but begins at ca. 80 °C lower than that for WS_2 nanostructures (530 °C, green line). The 80 °C difference between WS_2-coated MWCNs and WS_2 nanostructures in the oxidation process is possibly due to the fact that coating layers of WS_2 are thin and defective, allowing O_2 to diffuse into the layers easily. When the temperature reaches 600−700 °C, the uncoated MWCNs and particles (30−40% overall) begin to oxidize. This process accelerates when the temperature is raised to ca. 830 °C, the WS_2 coatings being continuously converted into WO_3.[20,21] At 900 °C, the uncoated MWCNs and carbon particles

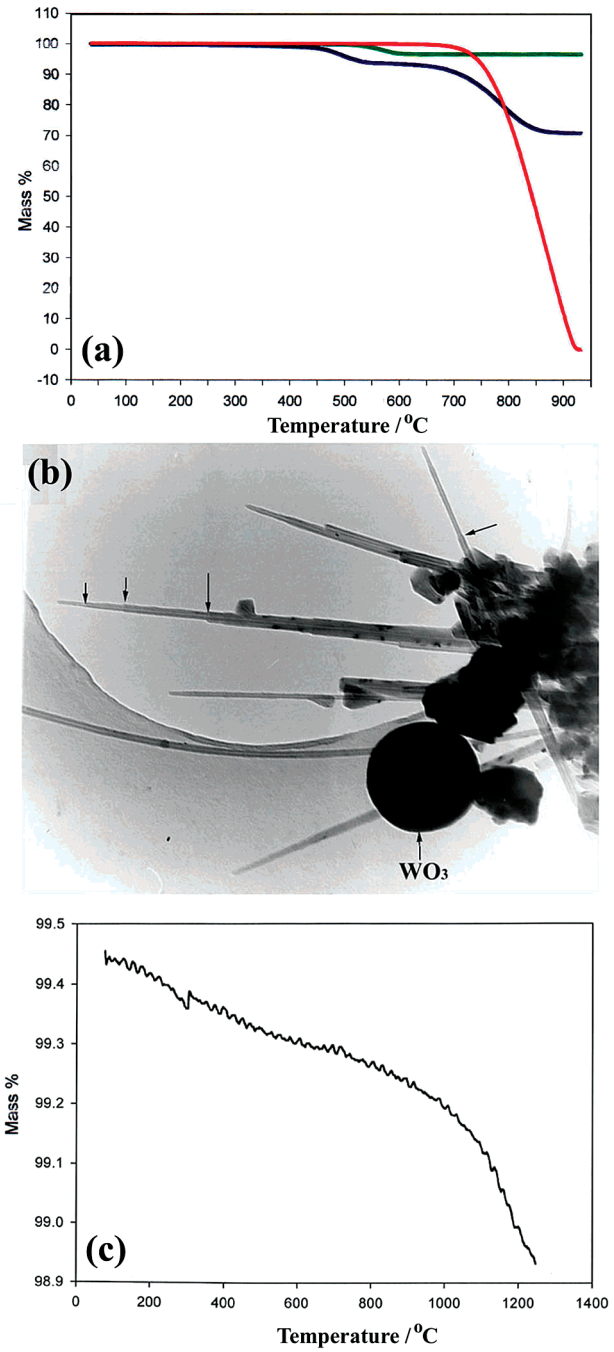

Figure 9. (a) TGA profiles for MWCNs (red line), WS_2-nanostructures (green line), and WS_2-coated MWCNs (blue line) conducted at a heating rate of 10 K min^{-1} in air. (b) HRTEM image of WS_2-coated MWCNs after TGA analysis. The MWCNs surfaces are mostly clean and are thinned due to oxidation (arrows). Black particles are also observed and EDX reveals that they consist predominantly of WO_{3-x}. (c) TGA profile displaying the stability of WS_2-coated MWCNs, heated to 1250 °C in Ar.

are fully oxidized and the WS_2 to WO_3 conversion is complete. The onset of oxidation of MWCNs, which are partly coated with WS_2, should occur at a slightly higher temperature than that for uncoated MWCNs, possibly between 800 and 900 °C. To test the thermal stability of WS_2-coated MWCNs, a sample was heated in an argon flow to 1220 °C, i.e. to just below its decomposition temperature of 1250 °C. The TGA record shows a minor mass loss of ca. 0.4% at 1220 °C

(19) Ebbesen, T. W.; Ajayan, P. M.; Hiura, H.; Tanigaki, K. *Nature* **1994**, *367*, 519.
(20) Hu, W. B.; Zhu, Y. Q.; Hsu, W. K.; Chang, B. H.; Terrones, M.; Grobert, N.; Terrones, H.; Hare, J.; Kroto, H. W.; Walton, D. R. M. *Appl. Phys. A* **2000**, *70*, 231.
(21) Zhu, Y. Q.; Hu, W. B.; Hsu, W. K.; Terrones, M.; Grobert, N.; Hare, J. P.; Terrones, H.; Kroto, H. W.; Walton, D. R. M. *Chem. Phys. Lett.* **1999**, *309*, 327.

(Figure 9c). TEM of the product showed that WS_2-coated MWCNs are still intact after heat treatment. The minor mass loss (0.4%) is possibly due to the small quantity of volatile amorphous WO_{3-x}[2,3] which was initially attached to the WS_2-coated MWCNs (Figure 1a).

Formation Mechanism for WS_2. The following factors are involved in the formation of WS_2 layers on MWCNs: (a) the MWCN geometry, particularly at the tube tips, (b) interactions between the carbon nanotube surface and coating material, and (c) the morphology and reorganization of amorphous WO_3 into hexagonal phase WS_2.

MWCN Geometry. The structure of WS_2 coating the MWCN body is similar to that found for WS_2 nanotubes,[2,3] although MWCNs with diameters < 5 nm exhibited incomplete WS_2 coating. This finding suggests that closure of WS_2 layers for low diameters may be difficult,[22] compared with that of carbon networks. Unlike closure by pentagonal ring disinclination in carbon networks, lattice vacancies are used for closure in WS_2 nanotubes.[5,6,23] However, the curvature created by lattice vacancies is limited[23] and so WS_2 nanotube tips or fullerene-like particles are mostly polyhedral,[2−6] whereas the tips of MWCNs are often conical or polyhedral, e.g. Figure 1d.[24] Partial as well as full WS_2 coating of various MWCN tips (e.g. Figure 1a,d) have frequently been observed. No specific MWCN tip geometry is found to be favorable for WS_2 coating. This finding implies that the WS_2 coating is not limited by the MWCN tip geometry, and that the axial flexibility of WS_2 is comparable with that of the C plane in the diameter range of 5−40 nm, based on the TEM investigations. The part WS_2 coating of the MWCN tips is mainly due to incomplete WO_{3-x} coating of MWCNs, prior to pyrolysis in an H_2S atmosphere (Figure 1a). We find that the incomplete WO_3 coating is apparent at the MWCN tips, which explains the presence of less WS_2 coating in the tube tips.

Substrate-Coat Interactions. Before its conversion to WS_2, WO_3 was deposited on the surface of the MWCNs (Figure 1a). When the WS_2 layers are formed, the innermost layer lies ca. 4.4 Å above the outermost layer of the MWCN surfaces; this value is somewhat greater than 3.4 Å, as found previously in C−MoS_2 and C−WS_2 materials.[9] The MWCNs provide a geometric template for the WS_2 coating process although the helicity, according to ED measurements, is not obviously related.

WO_3 Morphology. We assume that after reduction of WO_3 to WO_{3-x}, the rate of diffusion of H_2S into a coating of WO_{3-x} is faster than into crystalline WO_{3-x}. This is due to the thin, defective amorphous WO_{3-x} structure of the coating. It is therefore possible that the innermost and outermost WS_2 layers may form more-or-less simultaneously. Figure 10 shows the possible formation sequences for WS_2 from an uneven distribution of WO_3 supported by a MWCN. The first sequence (A) depicts an outward growth mechanism. H_2S diffuses through

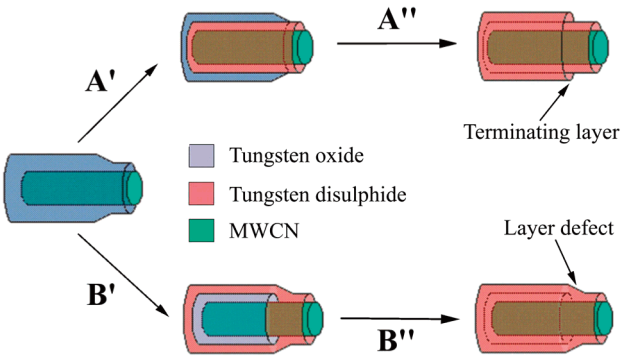

Figure 10. A model of possible sequences for the formation of layered WS_2 starting from an uneven distribution of WO_3 on the MWCN surface via (A) an outward and (B) an inward growth mechanism.

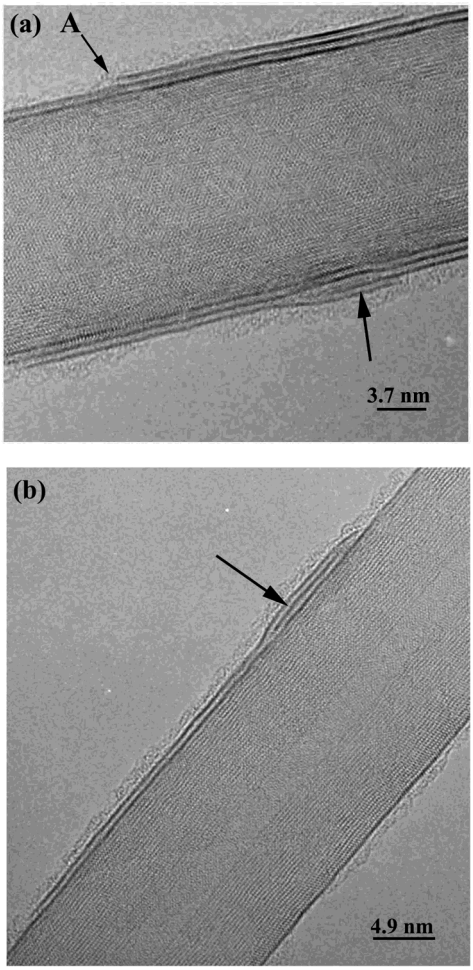

Figure 11. HRTEM image of WS_2-coated MWCNs exhibiting WS_2 layer defects (arrows).

the thin, defective WO_3 layers and a WS_2 tube forms directly around the carbon nanotube core (Step A′). The remaining outer WO_{3-x} is then converted into an outer-terminating WS_2 layer (Step A″) consistent with HRTEM images (Figures 1d and 11a, arrows A). The second sequence shows an inward growth mechanism, typically associated with the formation of separate WS_2 nanotubes.[2,3] As the WO_3 thickness decreases along the MWCN, the forming WS_2 layer will contain a lattice defect in order to obtain curvature along the MWCN axis in accordance with the template effect (Step B′).

(22) Seifert, G.; Terrones, H.; Terrones, M.; Jungnickel, G.; Frauenheim, T. *Phys. Rev. Lett.* **2000**, *85*, 146.
(23) Margulis, L.; Salitra, G.; Tenne, R.; Talianker, M. *Nature* **1993**, *365*, 113.
(24) Iijima, S.; Ichihashi, T.; Ando, Y. *Nature* **1992**, *356*, 776.

H_2S then diffuses through the outer WS_2 layers and converts the remaining WO_{3-x} into an internal terminating WS_2 layer (Step B″), also observed during the HRTEM investigation (Figure 3a, arrow A). Figure 11 shows WS_2-layered dislocations, in which an extra layer is sandwiched between continuous layers (arrows, Figure 11a,b). This type of dislocation is consistent with the formation sequences described above and has been observed previously.[5]

Powder XRD shows that the WO_3 precursor exhibits a monoclinic crystalline phase when the WO_3-coated MWCN sample is heated to 900 °C under nitrogen. Therefore, for the W atoms to adopt positions within the WS_2 hexagonal lattice, they must move from their sites within the monoclinic crystal. This phenomenon may account for continuous WS_2 layer formation even though the WO_3 distribution is usually uneven across the surface of the MWCN. A more detailed account of this concept will be given in a forthcoming publication.

Conclusions

We have demonstrated the facile way in which WO_3 can be deposited onto MWCN surfaces and converted to WS_2. Interestingly, this transformation converts disordered WO_3 coatings into layered WS_2 nanotubular sheaths. Characterization of the products shows only minor changes to the electronic structure of MWCNs. Hence the MWCNs act as a relatively inert template.

Due to its composite nature, we have improved the ability of MWCNs to withstand oxidation, which may find application as fire-retardant strengthening additives. Additionally, the 4.4-Å separation between the WS_2 and carbon layers may provide a discrete gap allowing the nanocomposite to be used as insulated nanowires. The electron transport measurements of these materials are currently under investigation.

Acknowledgment. We thank the Leverhulme Trust, EPSRC, ULIRS, and the Royal Society for financial support. We are grateful to D. Randall and J. Thorpe (University of Sussex) for assistance with the TEM analysis, to K. Brigatti (University of Sussex) for XRD analysis, to J. N. Hay (University of Birmingham) for assistance with high temperature TGA, and to J. Friend (The University of Manchester) for EPR measurements.

CM011282K